Journal of Materials Chemistry A

ROYAL SOCIETY OF CHEMISTRY

PAPER

View Article Online
View Journal | View Issue

Cite this: J. Mater. Chem. A, 2025, 13, 13100

Investigating transition metal crosstalk on SEI stability as a function of anode chemistry†

Sunggyu Yoon,[ab] Sung-Jin Chang,[c] Kangwoo Ahn*[d] and Minkyu Kim *[ab]

Received 22nd November 2024
Accepted 24th March 2025

DOI: 10.1039/d4ta08301f

rsc.li/materials-a

This study explores the effects of transition metal (TM) ions—Ni, Co, Mn, and Fe—on the solid-electrolyte interphase (SEI) formation and electrochemical behavior of graphite and silicon (Si) anodes in lithium-ion batteries (LIBs). Graphite anodes accumulate significantly more TM ions due to their higher electronic conductivity, which accelerates the hydrolysis of $LiPF_6$ salt during SEI formation, resulting in a less stable SEI and reduced cycle life. Si anodes, on the other hand, exhibit lower TM ion deposition, but TM ions promote the formation of an organic-rich SEI in the inner layer and accelerate $LiPF_6$ hydrolysis in the outer layer, increasing parasitic reactions and potentially shortening calendar life. Among the TM ions, Mn—though often regarded as particularly harmful—was found to be less detrimental than Ni and Co. Overall, the study demonstrates that the influence of TM crosstalk is highly dependent on both the anode material and the specific TM ions involved. These findings underscore the importance of tailoring strategies to mitigate TM ion effects in order to improve SEI stability and enhance the electrochemical performance of LIBs, which is essential for the development of high-performance, next-generation LIBs.

1. Introduction

Crosstalk in lithium-ion batteries (LIBs), which refers to chemical or electrochemical side reactions at one electrode that affect the properties of the other electrode, is a critical issue due to its significant impact on cell performance, safety, and cycle life.[1,2] A well-known example of this phenomenon is transition metal (TM) crosstalk. During charge and discharge cycles, TM ions dissolve from the cathodes and migrate to the anodes, where they significantly influence the solid electrolyte interphase (SEI) chemistry. Understanding the effects of TM crosstalk on the SEI of anode materials is essential for the development of high-performance LIBs.[1,3–14]

Numerous studies have focused on the impact of TM crosstalk in graphite-based batteries.[1,3–6] Although the specific mechanisms of TM crosstalk vary among reports, there is a consensus that TM ions deposited on the graphite anode negatively affect SEI stability by forming metallic species.[15] These metallic species can enhance electron conduction, leading to further electrolyte decomposition, increased impedance, surface parasitic reactions, cracking, and the formation of pores in the SEI layers of the graphite anode.[5,16,17] Therefore, mitigating TM dissolution and crosstalk behavior in conventional graphite-based batteries is crucial for achieving optimal electrochemical performance.

Recently, the demand for batteries with higher energy densities has driven a shift from graphite to silicon (Si) anodes. Si's exceptionally high gravimetric (3579 mA h g^{-1} for $Li_{15}Si_4$) and volumetric (2194 A h L^{-1} for $Li_{15}Si_4$) capacities make it a promising alternative for improving the energy density of LIBs.[18] Interestingly, several studies suggest that the mechanisms of TM crosstalk differ between Si and graphite anodes.[19–22] For instance, Kim *et al.* systematically compared the effects of TM crosstalk on the SEI of Si anodes as a function of cathode chemistry.[19,21,22] They found that when the Si anode was cycled with a $LiFePO_4$ cathode, a highly fluorinated SEI was formed, significantly reducing Li inventory loss. Understanding the mechanisms by which TM crosstalk affects SEI, and how these effects vary with anode chemistry, is essential for developing high-performance LIBs. While Si anodes offer significant potential for higher energy density, the effects of TM crosstalk on their SEI formation remain underexplored, compared to the well-established knowledge on graphite anodes.

This study aims to elucidate the behaviors of various TM ions (Ni, Co, Mn, and Fe) in relation to SEI formation on both graphite and Si anodes. Using time-of-flight secondary ion mass spectrometry (ToF-SIMS) and X-ray photoelectron spectroscopy (XPS), we examined the differential effects of these ions on SEI structure and composition. Based on the SEI results, we further

[a]Department of Chemistry, Inha University, 100 Inha-ro, Michuhol-gu, Incheon, 22212, Republic of Korea. E-mail: minkyu.kim@inha.ac.kr
[b]Department of Chemistry and Chemical Engineering, Inha University, 100 Inha-ro, Michuhol-gu, Incheon, 22212, Republic of Korea
[c]Center for Analysis and Evaluation, National Nanofab Center, Deajeon 34141, Republic of Korea
[d]Pohang Accelerator Laboratory (PAL), Pohang University of Science and Technology (POSTECH), Pohang, Gyeongbuk 37673, Republic of Korea. E-mail: ariel797@postech.ac.kr

† Electronic supplementary information (ESI) available. See DOI: https://doi.org/10.1039/d4ta08301f

investigated how these changes impact the electrochemical properties of each anode material. Through this approach, we aim to provide a comprehensive understanding of how TM crosstalk affects the performance of LIBs with different anode chemistries. Specifically, we found that TM ions in graphite primarily accelerate the hydrolysis of $LiPF_6$ in the inner SEI layer, which negatively impacts cycle life performance. In contrast, for the Si anode, TM ions lead to the formation of an organic-rich SEI in the inner layer and accelerate the hydrolysis of $LiPF_6$ in the outer SEI layer. This, in turn, results in significant parasitic reactions with the electrolyte, potentially affecting the calendar life of the battery. We also found that Mn ions, which are often considered highly detrimental, were less harmful compared to Ni and Co ions. This reduced impact may be attributed to Mn's lower tendency to deposit on anode electrodes.

Therefore, this study clearly suggests that the impact of TM crosstalk differs significantly depending on anode chemistry and types of TM ions, highlighting the need for a deeper understanding of the interactions between TM ions and various anode materials. Such insights are crucial for developing strategies to mitigate the negative effects of TM crosstalk on SEI stability and electrochemical performance, which is essential for advancing next-generation LIBs.

2. Result

2.1. The behaviors of deposition of TM ions as a function of anode chemistry

To investigate the effects of TM ions on the SEI of anode materials, various electrolyte samples were prepared containing different types of TM salts, specifically transition metal acetylacetonate ($TM(acac)_2$), at varying concentrations. These electrolytes were then used with graphite or Si anodes, which were cycled for three cycles at a 0.05C rate to form the SEI. To assess the effect of the anion in the TM salts, the graphite and Si electrodes were also cycled with electrolytes containing Li(acac), as shown in Fig. S1.† Fig. S1† demonstrated that the voltage *vs.* capacity curves and differential capacity curves (dQ/dV) of the graphite and Si cells with electrolytes containing Li(acac) were nearly identical to those of the cells without Li salt. This indicates that the anion in the TM salts does not significantly impact the electrochemical properties of either anode.

The first cycle coulombic efficiency provided key insights into the extent of electrolyte decomposition associated with SEI formation. Fig. 1a displays the voltage *vs.* capacity curves for graphite electrodes with and without TM salts in the electrolytes during the first cycle of the formation process. The corresponding differential capacity curves (dQ/dV) are shown in Fig. 1b. The inclusion of TM salts in the electrolytes led to additional peaks in Fig. 1b, likely due to side reactions involving TM ion deposition.[23] As a result, the first cycle coulombic efficiencies of the electrodes with TM-containing electrolytes were lower than those of electrodes without any salts (Fig. 1c): No salt: 86.9%, Ni salt: 77.6%, Co salt: 62.5%, Mn salt: 73.8%, and Fe salt: 52.4%. The significant variation in efficiencies among different TM ions suggests that the impact of TM ion deposition on SEI formation was dependent on the specific type of TM ion. After the first cycle, the coulombic efficiencies of all electrodes increased rapidly. Additionally, after SEI formation, the cells were disassembled, the same amount of TM salts was added again, and the cells were reassembled and cycled for three more cycles. This led to another significant drop in coulombic efficiencies (Ni salt: 86.7%, Co salt: 66.2%, Mn salt: 79.6%, and Fe salt: 51.9%). This can be explained by the dynamic behavior of the SEI and the role of TM ions. During the initial cycles, the SEI forms and stabilizes, leading to a gradual increase in coulombic efficiency as parasitic reactions such as electrolyte decomposition are mitigated. However, after reassembly with the addition of TM salts, newly introduced TM ions promote side reactions, including their redeposition on the electrode surface, temporarily destabilizing the SEI and causing a significant drop in coulombic efficiency. With further cycling, the SEI gradually reforms and stabilizes, reducing side reactions and allowing the coulombic efficiency to recover. This indicates that even after SEI formation, the continuous dissolution and deposition of TM ions on the graphite electrode can lead to severe side reactions.

A similar trend was observed for the Si anode (Fig. 1d–f). The addition of TM salts to the electrolytes lowered the first cycle coulombic efficiencies compared to the Si electrode without salts, and additional dQ/dV peaks appeared (Fig. 1e): No salt: 64.5%, Ni salt: 62.6%, Co salt: 59.5%, Mn salt: 60.2%, and Fe salt: 58.4%. However, the decrease in efficiency due to TM ions was less pronounced in Si electrodes compared to graphite electrodes. As with the graphite cases, when TM ions were reintroduced, the efficiencies of each cell dropped again, reinforcing the idea that side reactions could persist if TM dissolution and deposition continue, even after SEI formation.

These results suggest that the impact of TM crosstalk varies significantly depending on the specific type of TM ion and the type of anode material used. To gain a deeper understanding, we further examined the behavior of TM ions, focusing on how the effects differ based on the type of TM ion and the anode material used.

We first compared the amount of TM ions per surface area (ppm m^{-2}) on graphite and Si electrodes after the SEI formation process in Fig. 2a, since the amount of deposition of TM ions could be critical to the electrochemical properties and SEI of anode materials. The results showed that the TM amounts on the Si electrodes were significantly lower than those on the graphite electrodes, despite the same TM ion concentration (10 mM) in the electrolyte.

Since reduction reactions likely drive the TM deposition process, graphite appears to be a more favorable substrate for TM ion reduction due to its higher electronic conductivity. To verify this, the electronic conductivity of graphite and Si was measured using chronoamperometry (see Materials and methods section), revealing a significant difference between the two materials, as shown in Fig. S2.† The graphite exhibited a conductivity of 9.9 S cm^{-1}, whereas the Si powder had a much lower conductivity of 9.5×10^{-6} S cm^{-1}.

Additionally, considering the compositional differences between the graphite and Si electrodes used in this study, we

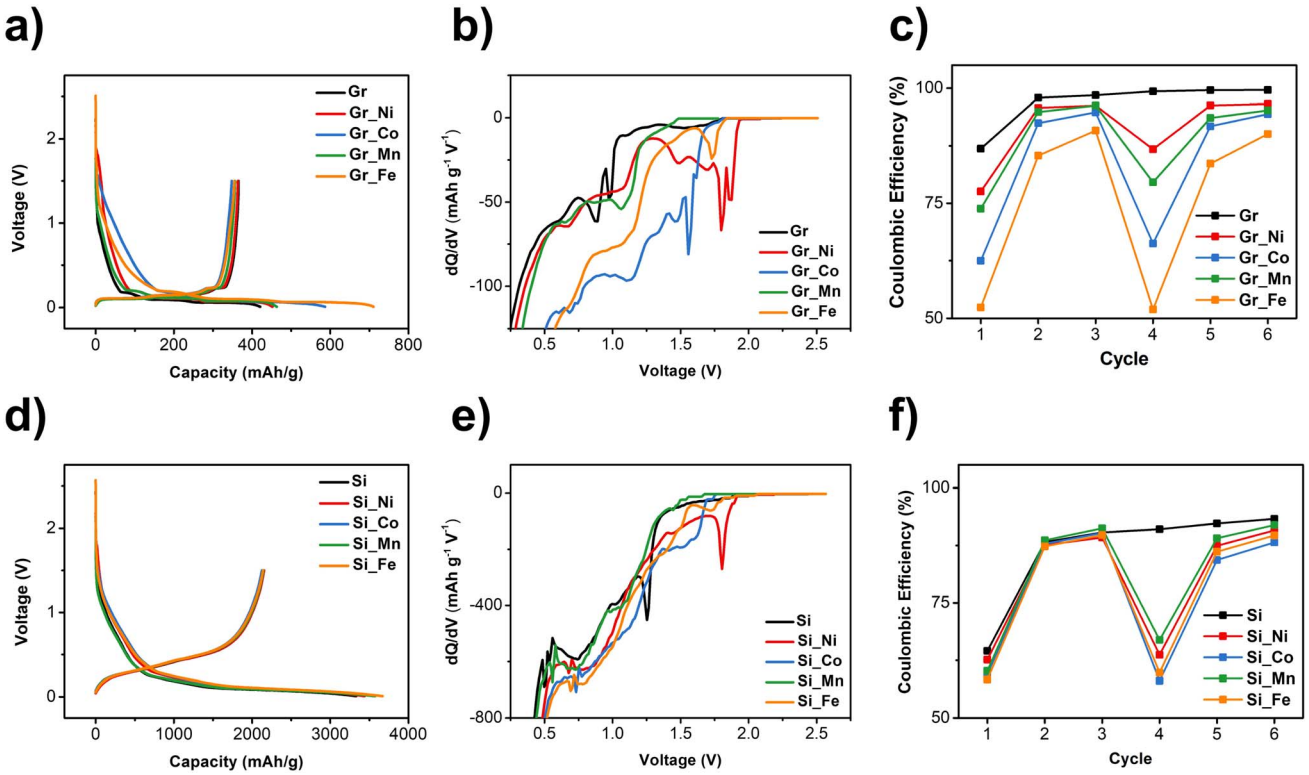

Fig. 1 Electrochemical performance during the formation process. Voltage *vs.* capacity curves during the first cycle for (a) graphite electrodes and (d) Si electrodes. Differential capacity *vs.* voltage curves during the first cycle for (b) graphite electrodes and (e) Si electrodes. Coulombic efficiencies of the initial three cycles and the subsequent three cycles after the extra addition of TM salts for (c) graphite electrodes and (f) Si electrodes.

evaluated whether variations in conductive agent content between these electrodes could influence TM deposition. To investigate this, we prepared an additional graphite electrode with the same composition as the Si electrode (active material : carbon black : binder = 6 : 3 : 1), as shown in Fig. S3.† The results confirmed that even under identical compositions, significantly more TM ions were deposited on the graphite electrode than on the Si electrode. This suggests that the difference in electronic conductivity between graphite and Si plays a more dominant role in influencing TM deposition than the contribution of carbon black alone.

The behavior also varies between different types of TM ions on the same anode material. Notably, the amount of Mn ions was significantly lower than that of other TM ions on both electrodes, indicating that Mn ion reduction is less favored. To our knowledge, these results provide the first comparison of TM ion deposition preferences on anode materials. Given the widely accepted view that Mn dissolution is particularly detrimental to SEI stability,[2,5,24–29] these findings suggest that investigating the amount of TM ion deposition on anode electrodes is essential for fully understanding crosstalk behaviors and their impacts.

Additionally, increasing the TM ion concentration in the electrolytes (from 10 mM to 30 mM to 50 mM) resulted in a rapid increase in TM ion deposition on the graphite electrode, indirectly supporting the notion that deposited TM ions facilitated further reduction reactions of dissolved TM ions in the electrolytes. These findings align with other reports suggesting that deposited TM ions act as an electron conduction antenna, leading to further reduction reactions of the electrolyte or TM ions.[15] In contrast, the amount of TM ion deposition on the Si electrodes rarely increased, indicating that deposited TM ions on the Si anode worked differently and did not facilitate further reduction of TM ions as seen with graphite.

2.2. The effects of TM crosstalk on SEI as a function of anode electrodes

2.2.1. The impact of TM crosstalk on SEI of graphite electrodes. TM ions deposited on anode electrodes significantly affected the electrolyte decomposition reactions, with impacts varying greatly depending on the specific type of TM ions and anode materials used. Five graphite electrodes were harvested after undergoing the SEI formation process. Gr_F was prepared in an electrolyte without any TM salt, while Gr_Ni_F, Gr_Co_F, Gr_Mn_F, and Gr_Fe_F were formed in electrolytes each containing 10 mM of Ni, Co, Mn, and Fe salts, respectively.

We first conducted scanning electron microscopy/energy dispersive spectroscopy (SEM/EDS) measurements on the harvested electrodes, as shown in Fig. S4.† The results indicate that the addition of TM salts significantly reduces the F atomic ratio, suggesting that TM salts strongly influence the decomposition of $LiPF_6$ during SEI formation.

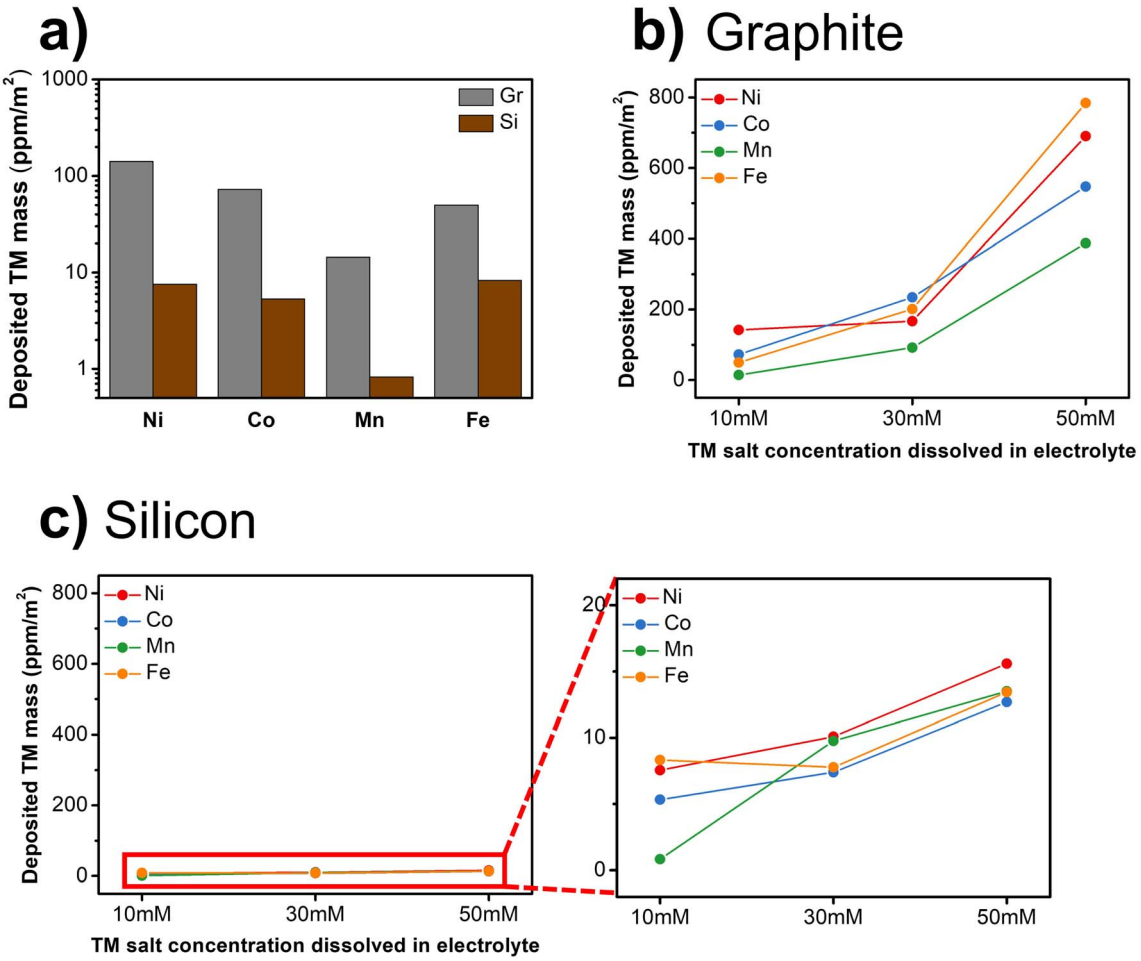

Fig. 2 (a) Amount of TM ions per surface area observed on graphite and Si electrodes after SEI formation when 10 mM of TM salts were added to electrolytes. Amount of TM ions per surface area on (b) graphite and (c) Si electrodes after SEI formation as a function of TM salt concentration in electrolytes. TM ions were measured using inductively coupled plasma optical emission spectroscopy (ICP-OES) or inductively coupled plasma mass spectrometry (ICP-MS). The surface area of each anode material was determined using the Brunauer–Emmett–Teller (BET) method. The results of BET are in Table. S1.†

To further deeply investigate the differences in SEI between each sample, ToF-SIMS analysis was then performed on these samples (see Fig. 3). Fig. 3a shows the normalized intensity of carbon species (C^-) as a function of sputter time for each sample. At the early stage of sputtering, the concentration of C^- was very low because graphite is covered by the SEI layer, but the concentration of C^- gradually increased as sputtering proceeded. Therefore, sputtering time could be assumed to directly relate to SEI layer thickness.[30,31] Based on this assumption, SEI thickness was defined as the sputtering time at which the normalized concentration of C^- reaches 0.8, marking the interface between the SEI layer and the underlying graphite electrode (Fig. 3a). Since sputter speed may vary across samples, we did not compare the SEI depth for each sample. Instead, each marker species was normalized to its maximum signal in the depth profiles (Fig. 3b–f).

The electrolyte used in this study consisted of $LiPF_6$ salt and carbonate-based organic solvents such as ethylene carbonate (EC) and ethyl methyl carbonate (EMC). Therefore, the intensity profiles of PFO^-, PO^-, PF^-, and LiF^-, LiF_2^- were used to represent the behavior of $LiPF_6$ salt decomposition, while the intensity profiles of C_2HO^-, CHO_2^-, CH_2^-, CH^- and C_2H^- indicated the behavior of carbonate-based organic solvent decomposition.[32,33]

For Gr_F, the SEI was divided into two distinct layers: the inner and outer SEI. The boundary between these layers was defined at the depth where species associated with the decomposition of $LiPF_6$ salt (PFO^-, PO^-, PF^-, and LiF^-, LiF_2^-) reached their local maximum intensities. In Gr_F, the intensity profiles of these species were closely similar. Starting from the innermost layer, their intensities steadily increased until peaking at the boundary, after which they gradually decreased. Therefore, the boundary between the inner and outer SEI could represent the point where $LiPF_6$ decomposition was most prevalent during SEI formation, and here, the boundary was specifically designated at the depth where the normalized intensity of LiF_2^- reached its maximum. In Gr_F, the inner and outer SEI layers were nearly equal in thickness. In contrast, the

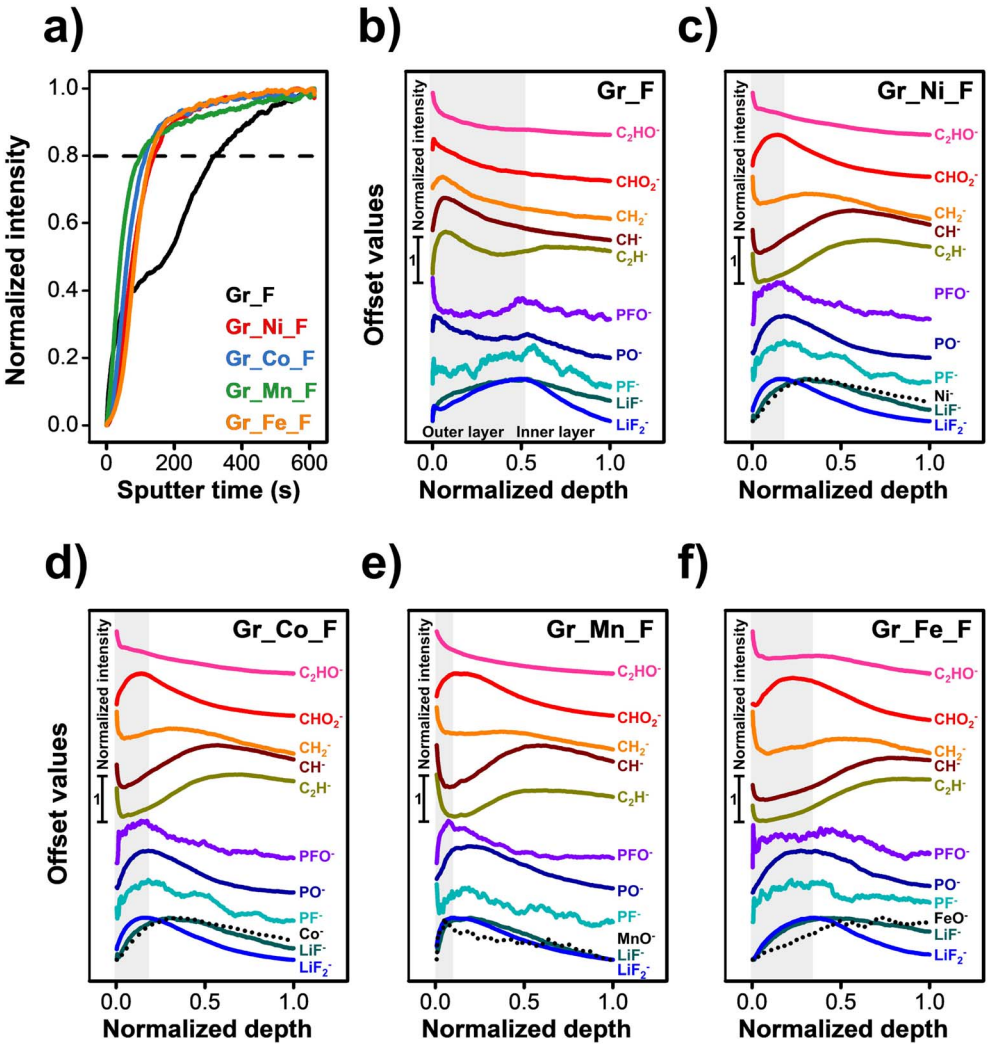

Fig. 3 ToF-SIMS analysis of harvested graphite electrodes after SEI formation. (a) Normalized intensity of C^- as a function of sputter time. Normalized intensity profiles of species related to the decomposition of organic solvents (C_2HO^-, CHO_2^-, CH_2^-, CH^-, and C_2H^-), and species associated with the decomposition of $LiPF_6$ salt (PFO^-, PO^-, PF^-, and LiF^-, LiF_2^-) as a function of normalized SEI depth for (b) Gr_F, (c) Gr_Ni_F, (d) Gr_Co_F, (e) Gr_Mn_F, and (f) Gr_Fe_F. The gray region represents the outer layer, while the non-colored region represents the inner layer. The intensity of each marker species was normalized to its maximum signals in the depth profiles.

intensities of species related to the decomposition of organic solvents (C_2HO^-, CHO_2^-, CH_2^-, CH^-, and C_2H^-) consistently increased as the SEI transitioned from the inner to the outer layer. This suggests that the decomposition of organic carbonate-based solvents was minimal in the early stages of SEI formation, but became more prominent as the SEI grew.

When TM salts were added to the electrolyte, the behavior of decomposition reactions exhibited significant differences compared to those in electrolytes without these salts (Fig. 3c–f). Firstly, the intensity profiles of species associated with $LiPF_6$ salt decomposition (PFO^-, PO^-, PF^-, and LiF^-, LiF_2^-) were notably altered, resulting in a substantial reduction in the width of the outer SEI layer. Secondly, the intensity profiles of species linked to $LiPF_6$ salt decomposition were highly synchronized with those of TM species, supporting the notion that the deposited TM ions had a major influence on the decomposition mechanism of $LiPF_6$ salt. Moreover, TM ions also significantly impacted the decomposition behavior of organic solvents. In Fig. 3b, species related to organic solvent decomposition (C_2HO^-, CHO_2^-, CH_2^-, CH^-, and C_2H^-) exhibited similar intensity profiles across the entire SEI for Gr_F. However, in Fig. 3c–f, some species showed contrasting behaviors. For example, while C_2HO^- and CHO_2^- maintained intensity profiles similar to those observed in Gr_F, the profiles for CH^- and C_2H^- exhibited opposite behavior compared to those in Gr_F. The intensities of these species decreased from the inner to the outer region, supporting the idea that decomposition behaviors of organic solvents were altered by TM ions on graphite electrode.

As a result of the effect of the deposited TM ions on the electrolyte decomposition behavior, the SEI chemistry was significantly altered when TM ions were added in electrolyte. XPS analysis was performed on harvested electrodes after SEI formation (Fig. 4). Additionally, another five graphite electrodes

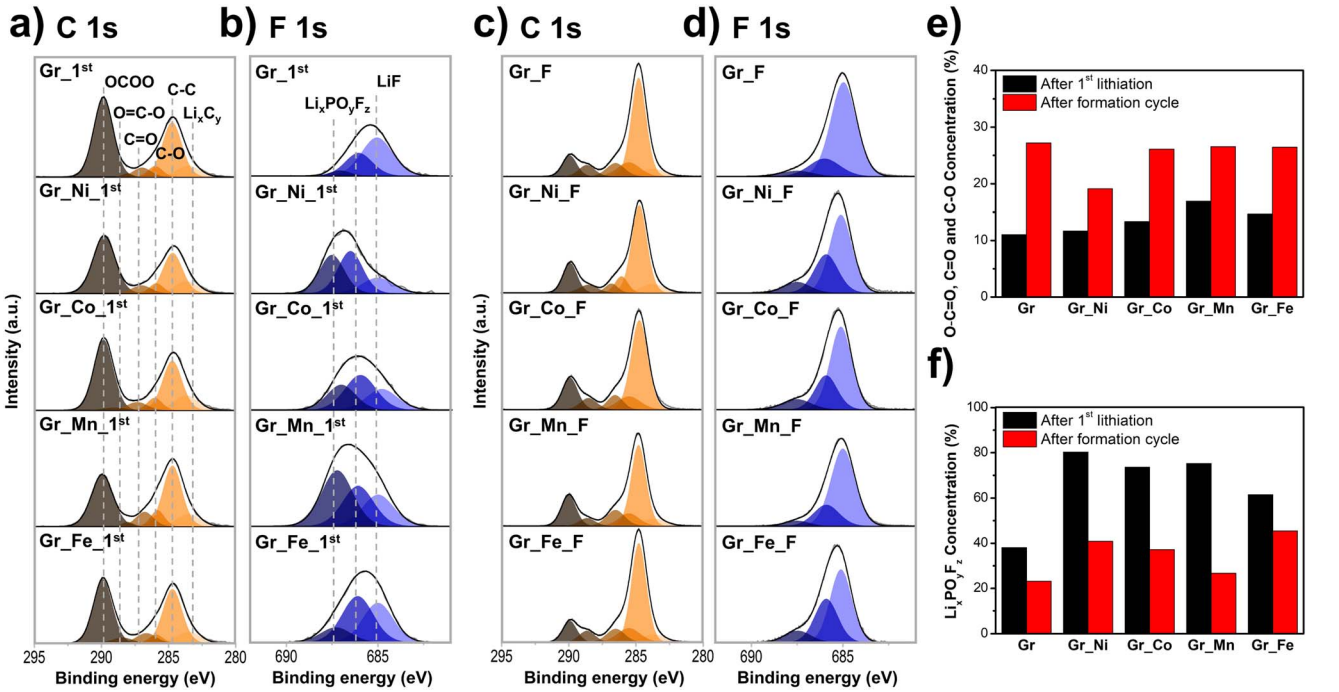

Fig. 4 XPS analysis of harvested graphite electrodes. (a) C 1s spectra and (b) F 1s spectra of the harvested graphite electrodes after the first lithiation. (c) C 1s spectra and (d) F 1s spectra of the harvested graphite electrodes after the SEI formation process. (e) Concentration of O–C═O, C═O, and C–O observed in C 1s spectra of the harvested graphite electrodes after the first lithiation and after the SEI formation process. (f) Concentration of $Li_xPO_yF_z$ observed in F 1s spectra of the harvested graphite electrodes after the first lithiation and after SEI formation.

were harvested after the first lithiation to examine the effects of TM ions on the early stage of SEI formation. Gr_1st was prepared after the first lithiation in an electrolyte without any TM salt, while Gr_Ni_1st, Gr_Co_1st, Gr_Mn_1st, and Gr_Fe_1st were formed in electrolytes containing 10 mM of Ni, Co, Mn, and Fe salts, respectively.

Fig. 4a shows the C 1s spectra of each sample harvested after the first lithiation. For Gr_1st, ether- and carbonate-based species (*e.g.*, C–O, C═O, O–C═O, and OCOO) were present in significant amounts, along with the lithiated carbon peak. Since the formation of ether- and carbonate-based species results from the electrochemical reduction of organic solvents, comparing the C 1s spectra suggests how SEI chemistry differs as a function of TM ions on the graphite electrode.[34,35] In this context, the C 1s spectra for each electrode do not show significant differences between them. Specifically, Fig. 4e compares the ether-based species (O–C═O, C═O, and C–O), which are indicative of organic compound formation in each sample,[34–37] showing that the concentrations remained consistent regardless of the type of TM salt used in the electrolyte or its absence. These findings suggest that the altered decomposition behavior of organic solvents, as observed in the ToF-SIMS results (Fig. 3), had no significant impact on the decomposition products and, consequently, the SEI chemistry of the graphite electrode. After SEI formation, the C 1s spectra (Fig. 4c and e) show that the concentration of ether-based species (O–C═O, C═O, and C–O) significantly increases for all samples, indicating that the formation of organic compounds was further accelerated.

In contrast, the F 1s spectra of each electrode harvested after the first lithiation exhibited significant differences (Fig. 4b), indicating that the decomposition products of $LiPF_6$ salt was largely influenced by the presence of TM ions on the graphite electrodes during early SEI formation stages. Compared with Gr_1st, the other harvested graphite electrodes exhibited a significant increase in the ratio of $Li_xPO_yF_z$ species (Fig. 4b and f). Given that the formation of $Li_xPO_yF_z$ species generally results from the hydrolysis reaction of $LiPF_6$ salt, this finding suggested that deposited TM ions on graphite electrodes acted as catalysts, accelerating the hydrolysis reaction, as widely reported.[38,39] After SEI formation, the F 1s spectra (Fig. 4d and f) showed that all samples had a lower ratio of $Li_xPO_yF_z$ compared to the electrodes harvested after the first lithiation shown in Fig. 4b. However, the electrodes formed with electrolytes containing Ni, Co, and Fe (Gr_Ni_F, Gr_Co_F, Gr_Fe_F) still had a higher concentration of $Li_xPO_yF_z$ compared to Gr_F and Gr_Mn_F.

In summary, TM ions on graphite electrodes altered the decomposition of some organic solvents, though SEI chemistry for this decomposition remains unchanged. Additionally, TM ions accelerated the hydrolysis of $LiPF_6$ salt during the early stages of SEI formation. However, their impact on the SEI is less severe for the outer layer compared to the inner layer. This aligned with the sharp decline in coulombic efficiency observed during the first cycle due to TM ion deposition, underscoring the detrimental impact of TM dissolution on SEI chemistry.

2.2.2. The impact of TM crosstalk on SEI of Si electrodes. To investigate the effects of TM ions on Si, five Si electrodes

were harvested after three cycles at 0.05C during the SEI formation process. Si_F was formed in an electrolyte without any TM salt, while Si_Ni_F, Si_Co_F, Si_Mn_F, and Si_Fe_F were formed in electrolytes each containing 10 mM of Ni, Co, Mn, and Fe salts, respectively. SEM/EDS results for the harvested electrodes, shown in Fig. S5,† indicate that the O element exhibited higher intensity and an increased atomic ratio in the presence of TM salts. Additionally, a noticeable reduction in the F element was observed with TM salt addition. These findings suggest that, in the Si electrode, TM salts significantly influence the decomposition of both $LiPF_6$ salt and organic solvents.

ToF-SIMS analysis was further conducted on these samples (see Fig. 5). As with the graphite electrodes, the SEI thickness was defined as the sputtering time at which the normalized concentration of Si^- reaches 0.8 (Fig. 5a).[19] Then, each marker species was normalized to its maximum signal in the depth profiles (Fig. 5b–f).

For Si_F (Fig. 5b), the overall intensity profiles for each species differed significantly from those of Gr_F. Unlike Gr_F (Fig. 3b), the intensities of for CH^- and C_2H^- were significantly higher in the innermost SEI region and decreased continuously from the inner to the outer region, indicating that organic solvent decomposition behaviors significantly differed from those for graphite electrode. Interestingly, the intensity profiles of species related to the decomposition of organic solvents (C_2HO^-, CHO_2^-, CH_2^-, CH^-, and C_2H^-) were similar to the profiles of graphite with TM ions (Fig. 3c–f).

When TM salts were added to the electrolyte (Fig. 5c–f), the intensity profiles of species associated with $LiPF_6$ salt decomposition were highly synchronized with those of the TM species, similar to what we observed for the graphite electrode samples (Fig. 3). This supports the idea that the deposited TM ions also had a significant influence on the decomposition mechanism of $LiPF_6$ salt for the Si electrode. On the other hand, no significant

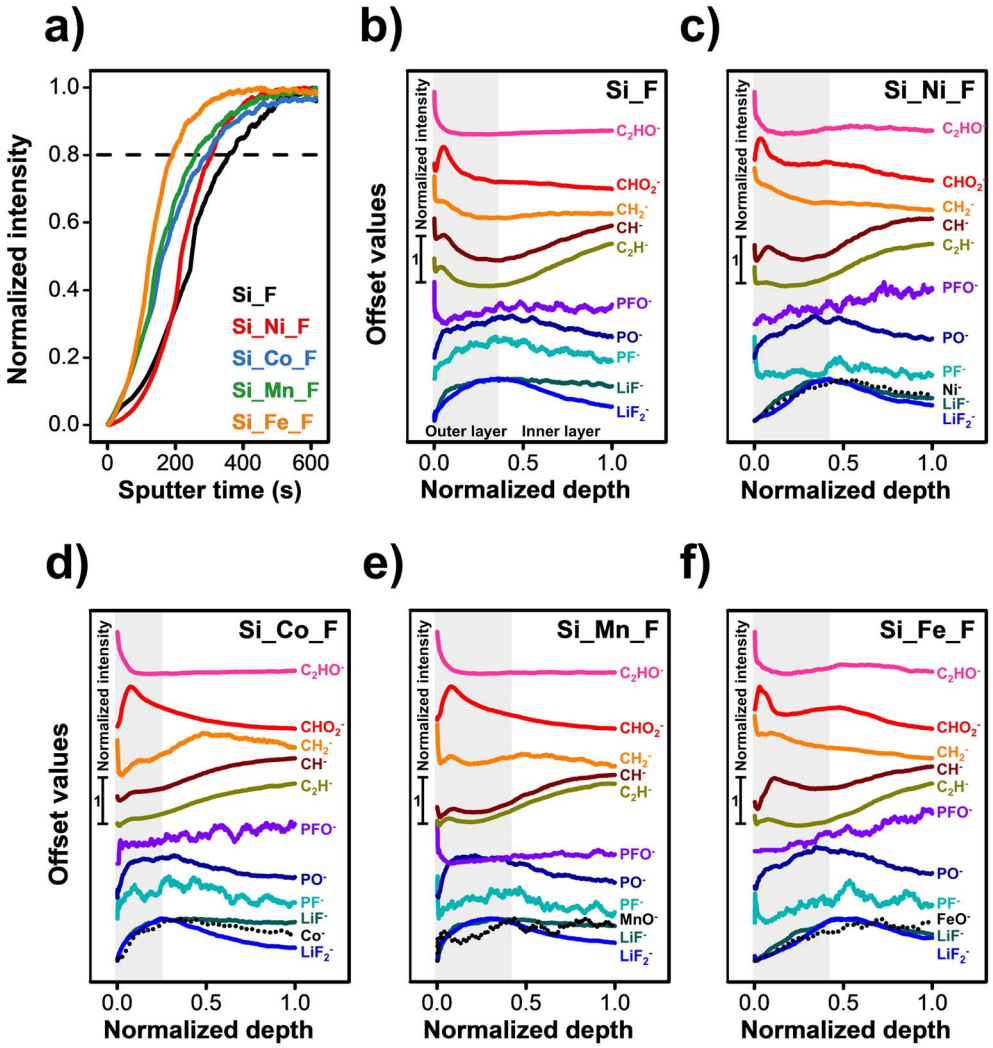

Fig. 5 ToF-SIMS analysis of harvested Si electrodes after SEI formation process. (a) Normalized intensity of Si^- as a function of sputter time. Normalized intensity profiles of species related to the decomposition of organic solvents (C_2HO^-, CHO_2^-, CH_2^-, CH^-, and C_2H^-), and species associated with the decomposition of $LiPF_6$ salt (PFO^-, PO^-, PF^-, and LiF^-, LiF_2^-) as a function of normalized SEI depth for (b) Si_F, (c) Si_Ni_F, (d) Si_Co_F, (e) Si_Mn_F, and (f) Si_Fe_F. The grey region represents the outer layer, while the non-colored region represents the inner layer. The intensity of each marker species was normalized to its maximum signals in the depth profiles.

changes were observed in the intensity profiles of species related to the decomposition of organic solvents (C_2HO^-, CHO_2^-, CH_2^-, CH^-, and C_2H^-) for the other samples (Si_Ni_F, Si_Fe_F, Si_Co_F, Si_Mn_F).

XPS analysis was also performed on harvested Si electrodes after the first lithiation process and after SEI formation in electrolytes with or without TM salts. The harvested Si electrodes after the first lithiation are hereafter referred to as Si_1st, Si_Ni_1st, Si_Co_1st, Si_Mn_1st, and Si_Fe_1st, following the same naming convention as the graphite electrodes.

Fig. 6a shows the C 1s spectra of Si electrodes harvested after the first lithiation. Unlike the harvested graphite electrodes (Fig. 4), the deposition of TM ions on the Si electrode significantly influenced the decomposition products of organic carbonate-based solvents, leading to changes in the SEI chemistry of the Si electrode. Fig. 6a and e show that, compared to the C 1s spectra of Si_1st, the concentration of OCOO species was largely suppressed, while the concentration of ether-based species (O–C=O, C=O, C–O) increased for the other harvested electrodes (Si_Ni_1st, Si_Co_1st, Si_Mn_1st, and Si_Fe_1st). Since OCOO species correspond to the formation of inorganic lithium carbonate (Li_2CO_3), while ether-based species (O–C=O, C=O, C–O) correspond to the formation of organic species,[34–37] these results suggest that relatively organic-rich SEI formed due to the deposited TM ions on Si electrodes during the early SEI formation stages, compared to Si_1st. For the F 1s spectra (Fig. 6b and f), Si_Ni_1st, Si_Co_1st, and Si_Fe_1st exhibited a relatively higher concentration of $Li_xPO_yF_z$, indicating that Ni, Co, or Fe ions deposited on Si electrodes accelerated the hydrolysis reaction of $LiPF_6$. However, this effect was less significant for Si electrodes compared to their impact on graphite electrodes.

After SEI formation, the F 1s spectra showed an increased concentration of $Li_xPO_yF_z$ species for all samples, suggesting that the hydrolysis reaction was further accelerated as SEI formation continued (Fig. 6d and f). This is the opposite trend to what was observed for graphite electrodes. Among them, Si_Ni_F exhibited a much higher ratio than the others, while Si_Mn_F showed the most moderate difference compared to Si_F. This could be because the amount of Mn ion deposited on the Si electrode was the lowest among all TM ions.

In summary, TM ions on Si electrodes accelerated the formation of organic-rich SEI during the early stages of SEI formation. Additionally, in contrast to graphite electrodes, where hydrolysis of $LiPF_6$ was significantly observed in the inner SEI layer, the hydrolysis of $LiPF_6$ in Si electrodes was less significant in the inner layer but became more prevalent in the outer layer when TM ions were present in the electrolyte.

2.3. The effect of TM deposition on the electrochemical stability of SEI depending on anode materials

To investigate the influence of TM salts on electrochemical properties of the anode materials, we performed a potentiostatic hold test in Fig. 7. During the potentiostatic hold test, surface parasitic reactions between graphite or Si and the electrolyte are accelerated, becoming more pronounced as the SEI stability of the material decreases. Since surface parasitic

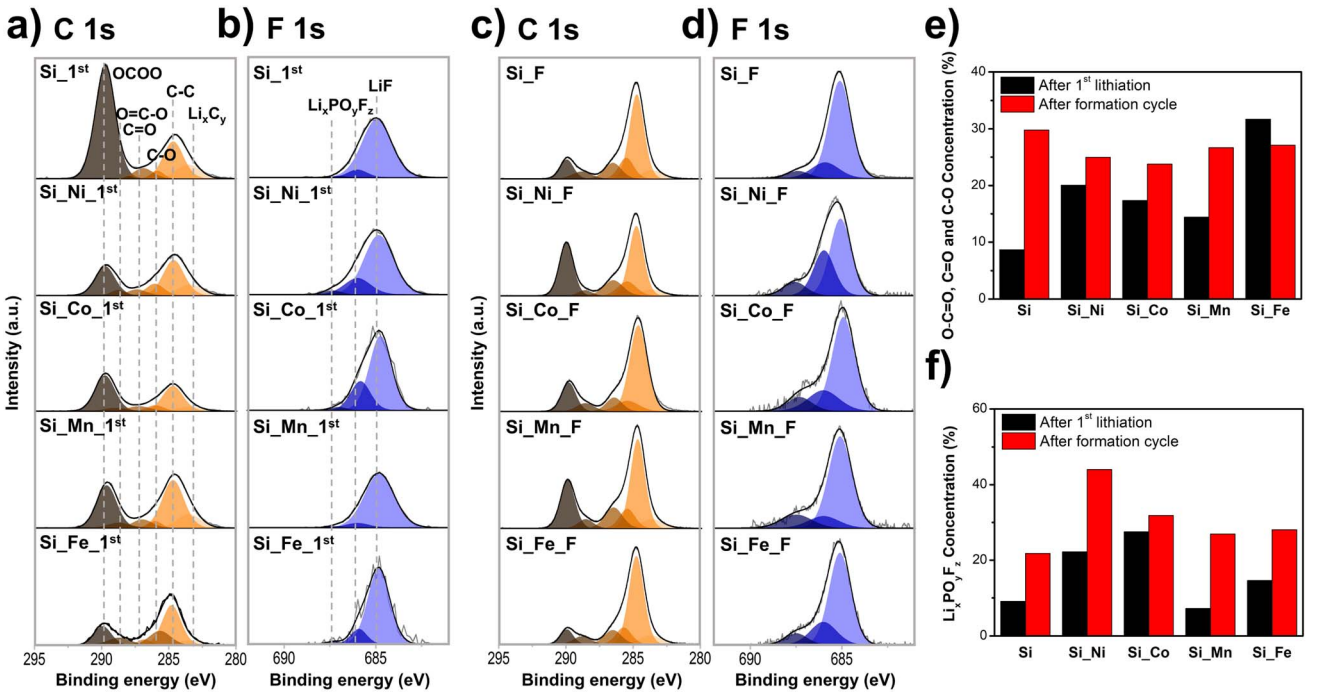

Fig. 6 XPS analysis for harvested Si electrodes. (a) C 1s spectra and (b) F 1s spectra of the harvested Si electrodes after the first lithiation. (c) C 1s spectra and (d) F 1s spectra of the harvested Si electrodes after the SEI formation process. (e) Concentration of O–C=O, C=O, and C–O observed in C 1 s spectra of the harvested Si electrodes after the first lithiation and after the SEI formation process. (f) Concentration of $Li_xPO_yF_z$ observed in F 1s spectra of the harvested Si electrodes after the first lithiation and after SEI formation.

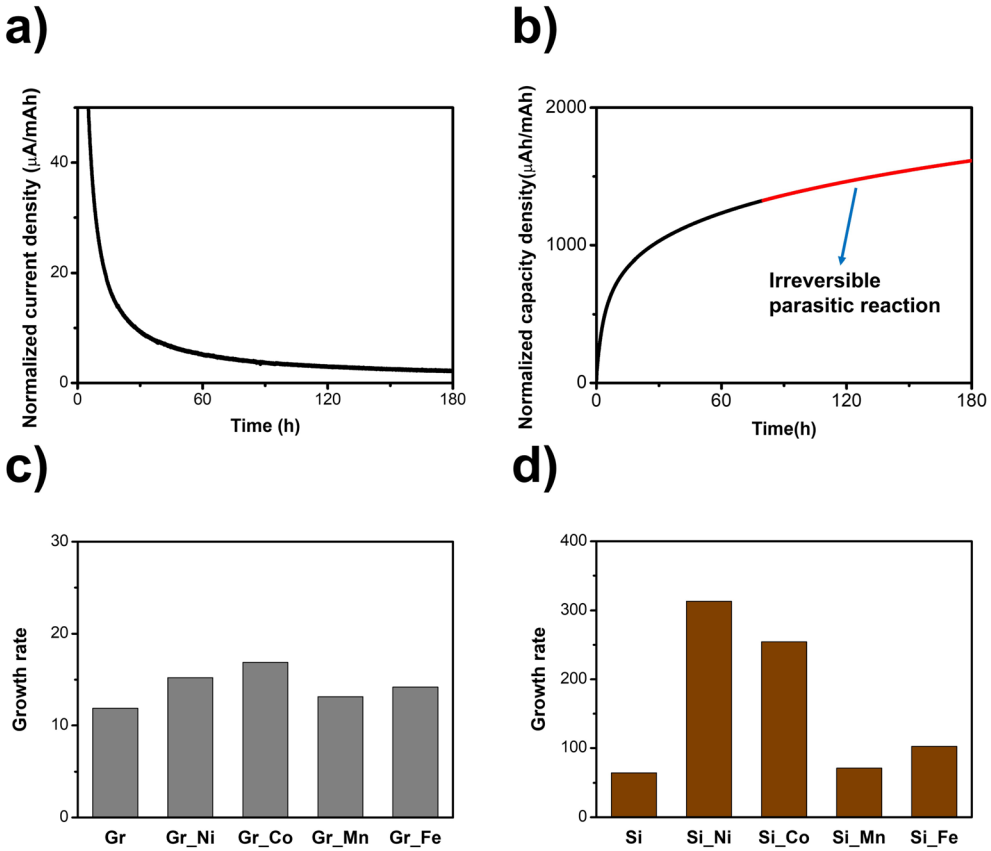

Fig. 7 (a) Normalized current density *vs.* time curve of Si electrode in an electrolyte without TM salts during potentiostatic hold test for 180 hours at 0.1 V. The current density was normalized to the lithiation capacity measured immediately before the potentiostatic hold test. (b) Normalized capacity density *vs.* time curve of Si electrode in an electrolyte without TM salts, integrated from the curve in (a). (c) The growth rates of irreversible capacity (b_1) for each graphite electrodes with/without TM salts. (d) The growth rates of irreversible capacity (b_1) for each Si electrodes with/without TM salts.

reactions with the electrolyte significantly contribute to the degradation of the calendar life of active materials, the potentiostatic hold test has recently been adopted as an early indicator for evaluating the calendar life of anode materials.[19,40–42] For this purpose, the cells undergoing formation process with or without TM salts in electrolytes were further lithiated to 0.1 V, followed by a potentiostatic hold at 0.1 V for 180 hours to measure leakage current.[43] Since lithiation capacity varied across samples, the current values were normalized by dividing by the capacities lithiated to 0.1 V. Fig. 7a displays the normalized current density *vs.* time for the Si electrode without TM salts in the electrolyte. Initially, a large current was observed due to reversible lithiation reactions, which then rapidly decayed.[43] However, even after 180 hours, a relatively high current persisted, indicating ongoing electrochemical reactions due to parasitic interactions between the electrolyte and the Si surface, leading to electrolyte decomposition and Li-ion consumption.[43]

We integrated the curves in Fig. 7a to convert them into normalized capacity density *vs.* time (Fig. 7b). The early exponential growth in normalized capacity corresponds to reversible lithiation reactions. However, the persistent power-law growth observed at extended times reflects ongoing irreversible parasitic reactions, such as continuous electrolyte decomposition and SEI growth.[19] These reactions are directly linked to the b_1 parameter, which quantifies the rate of irreversible capacity growth. We fitted this data using a power-law equation ($a_1 + b_1 \times (\text{time})^{1/2}$) from 80 to 180 hours, following the methodology used in recently published works.[19] The parameter b_1, which represents the growth rate of irreversible capacity due to parasitic reactions, could serve as an indicator of SEI stability of anode material. The increase in b_1 values in the presence of TM ions indicates their strong catalytic role in promoting these irreversible reactions. This parameter could thus be used as an early indicator for assessing the calendar life of anode materials, as suggested in other reports.[19] The same tests were performed for the other samples, and the b_1 values are summarized in Fig. 7c (graphite electrodes with/without TM salts) and Fig. 7d (Si electrodes with/without TM salt).

Compared to the graphite electrode without TM salts, the b_1 value for the Si electrode without TM salts was significantly higher, indicating that the SEI on graphite was more stable than that on Si. Additionally, the introduction of TM ions into the electrolyte increased b_1 values for both materials, with a more pronounced effect on Si electrodes. For example, the b_1 value for graphite electrodes was highest when Co salt was added,

making it 2.3 times higher than that of graphite without any salts. In contrast, the maximum b_1 value for Si electrodes was observed when Ni salt was added, and it was 4.9 times higher than that of the Si electrode without any salts.

Furthermore, the Si electrodes with TM salts showed more pronounced differences depending on the specific TM salt used, compared to the graphite electrodes. For instance, Si electrodes with electrolytes containing Ni and Co ions exhibited a substantial increase in b_1 values, while Mn and Fe ions had a relatively lower impact. In Si electrodes, it has been reported that hydrolysis reactions can lead to the formation of an unstable SEI consisting of $Li_xPO_yF_z$ species, which in turn results in higher b_1 values.[19] Consequently, the elevated b_1 values observed in Si electrodes with electrolytes containing Ni and Co ions could be likely due to the significant formation of $Li_xPO_yF_z$ species in the outer layer of the SEI, as supported by the XPS analysis shown in Fig. 6.

We further investigated the impact of TM salts during cycle life tests. Fig. 8 shows the discharge specific capacity and coulombic efficiency over 100 cycles at 0.2C after the formation process. For graphite without TM salt (Fig. 8a), although the capacity observed in the early stage of the cycle test was slightly lower than the theoretical value (372 mA h g^{-1}), it continuously increased as the test progressed, eventually reaching values close to the theoretical limit, and then cycled stably for 100 cycles. The coulombic efficiencies during cycles followed a similar trend, as shown in Fig. 8b.

On the other hand, when TM salts were added (Fig. 8a and b), higher capacities were observed at the early stage of cycle test, likely due to significant side reactions. However, as cycling progressed, the reversible capacity steadily decreased, leading to a continuous decline in overall capacity throughout the 100 cycles. The coulombic efficiencies for the graphite electrodes with electrolytes containing TM salts were also lower throughout the entire test compared to the electrode without TM salts.

Interestingly, for Si electrodes (Fig. 8c and d), the coulombic efficiency did not differ as significantly as it did in graphite samples. In terms of capacity, Si electrodes with Ni or Co salts in electrolytes exhibited lower discharge capacities from the initial cycles compared to Si electrode without TM salt addition. On the other hand, Si electrode with Mn salts exhibited the lowest fading rate among all the tested cells. This was further supported by the results obtained under a cutoff voltage of 0.1 V, where the capacity fading of Si was significantly suppressed (Fig. S6†). All cells in Fig. S6† exhibit comparable coulombic

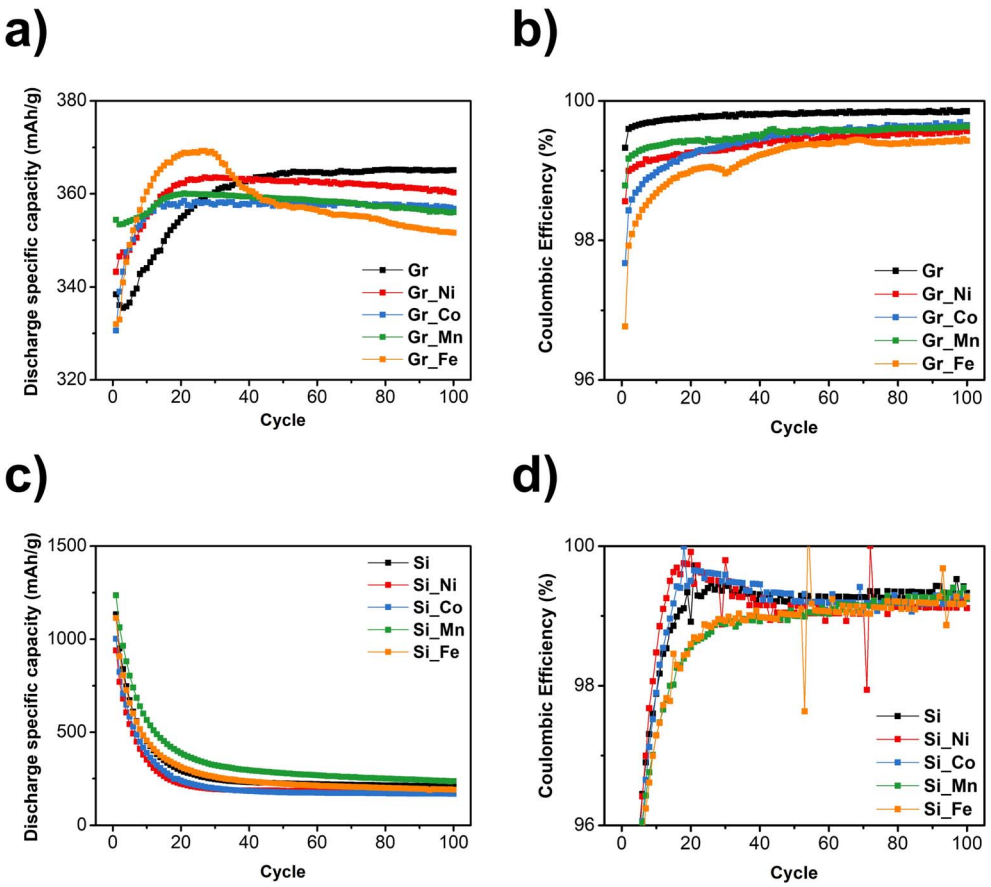

Fig. 8 Long-term cycling performance during 100 cycles at 0.2 C. Discharge specific capacity *vs.* cycle number for (a) graphite electrodes with/without TM salts and for (c) Si electrodes with/without TM salts. Coulombic efficiency *vs.* cycle number for (b) graphite electrodes with/without TM salts and for (d) Si electrodes with/without TM salts.

efficiencies, with some even showing improved cycle retention performance upon the addition of TM salts.

3. Discussion

3.1. Impacts of TM ions on SEI and electrochemical properties depending on anode material

Our study highlights the critical role of TM ion deposition in shaping the SEI and its subsequent effects on electrochemical performance, with these impacts strongly dependent on the anode material. Due to its preference for TM reduction, graphite electrodes exhibit significantly greater TM ion accumulation on their surfaces. This deposition promotes the hydrolysis of $LiPF_6$ salt, leading to the formation of inorganic species like $Li_xPO_yF_z$, which destabilize the inner SEI layer. These phenomena were confirmed by XPS and ToF-SIMS analyses (Fig. 3 and 4), which revealed elevated concentrations of these species in the presence of TM ions. Additionally, the deposited TM ions enhance electron conduction pathways, facilitating further electrolyte decomposition and parasitic reactions. This cascade of effects results in an unstable SEI that accelerates capacity fade, particularly during cycling, as evidenced by the decline in coulombic efficiency during the first cycle.

In contrast, Si electrodes exhibit significantly less TM ion deposition under similar conditions. However, TM ions still influence SEI formation by accelerating the development of an organic-rich SEI. Unlike in graphite electrodes, where hydrolysis of $LiPF_6$ predominantly affects the inner SEI layer, Si electrodes exhibit this reaction primarily in the outer SEI layer. This distinction reflects the material-specific behavior of TM ions and their effects on SEI chemistry.

These differences in the effects of TM crosstalk on SEI formation for Si electrodes, compared to graphite electrodes, lead to distinct impacts on their electrochemical properties. Potentiostatic hold tests revealed increased parasitic reaction rates in Si electrodes with TM ions, correlating strongly with calendar life degradation.[19,40–42] These results suggest that TM crosstalk significantly and negatively affects the calendar life of Si electrodes, while its impact on graphite electrodes is relatively less severe.

3.2. Impacts of different TM ions on SEI and electrochemical properties

The type of TM ion plays a crucial role in determining its impact on the SEI, with notable differences observed among ions such as Ni, Co, Mn, and Fe. Each of these ions interacts uniquely with the anode material and electrolyte, leading to distinct effects on the SEI's formation, composition, and stability.

While Mn ions are often considered highly detrimental due to their ease of dissolution from cathodes,[2,5,24] our study shows that Mn deposition on anode surfaces is less favored, resulting in lower concentrations and reduced impact on SEI stability compared to other TM ions. Consequently, Mn ions exhibit a relatively moderate influence on parasitic reactions and capacity fade. In contrast, Ni and Co ions significantly exacerbate parasitic reactions during potentiostatic hold tests, as reflected by higher b_1 values. Fe ions have the most pronounced negative effects on cycle life of graphite.

These findings suggest that both the reduction preferences of TM ions on electrode surfaces and their distinct effects on SEI stability and electrochemical properties must be carefully considered when designing strategies to mitigate TM crosstalk.

4. Conclusion

This study provides a comprehensive analysis of the impact of TM ions on the SEI and electrochemical properties, with a particular focus on the differences observed between graphite and Si electrodes. The findings highlight the significant role that the type of TM ion and the anode material play in determining the formation, composition, and stability of the SEI, as well as the overall cell performance.

For graphite electrodes, the superior electronic conductivity facilitates a greater accumulation of TM ions on the surface, accelerating hydrolysis reaction of $LiPF_6$ salt at the early stage of SEI formation. This results in a less stable SEI. This instability was particularly pronounced in the inner SEI layer, contributing to a rapid decline in capacity during cycle life tests.

In contrast, Si electrodes exhibit considerably lower TM ion deposition under similar conditions, suggesting a lower propensity for TM ion reduction on the Si surface. The primary effect of TM ions on Si electrodes is seen in the acceleration of the formation of organic-rich SEI in the inner SEI. Additionally, unlike graphite, Si electrodes show less significant hydrolysis of $LiPF_6$ in the inner SEI layer, with this reaction becoming more pronounced in the outer layer when TM ions are present. TM crosstalk was found to have a more pronounced effect on the extent of parasitic reactions during potentiostatic hold tests for Si electrodes, which could negatively affect the calendar life of Si-based batteries. However, the impact on cycle life was relatively less severe, with Si electrodes containing Mn salt even showing improved performance.

Additionally, the type of TM ion plays a critical role in determining its impact on SEI formation and electrochemical performance. While Mn ions are often considered highly detrimental due to their ease of dissolution from cathodes, our findings suggest that Mn has a less harmful impact on SEI stability and battery performance compared to Ni and Co ions. The differences in TM ion reduction preferences and their varied effects on SEI stability and electrochemical properties underscore the need to carefully consider TM crosstalk mechanisms.

In conclusion, this study demonstrates that the effects of TM crosstalk vary significantly depending on the anode chemistry and the specific TM ions involved. This highlights the importance of developing a more comprehensive understanding of how TM ions interact with different anode materials. Such insights are essential for devising strategies to mitigate the detrimental effects of TM crosstalk on SEI stability and electrochemical performance, which is crucial for advancing the development of next-generation LIBs. By systematically analyzing TM ion deposition behaviors and their impact on SEI

stability, this work offers valuable insights for designing high-performance LIBs with improved performance.

5. Materials and methods

Materials: In this study, Si was mechanically crushed using a planetary ball mill to reduce its particle size. Subsequently, both Si and graphite were pre-mixed with a conducting agent in a ball mill for 12 hours. Polyacrylic acid (PAA) was used as the binding agent. These materials were then mixed with *N*-methyl-2-pyrrolidone (NMP) in a paste mixer. The resulting mixed slurries were spread onto a copper current collector using a doctor blade. The compositions are presented in Table 1.

Cell (dis)assembly and testing

All electrochemical cell tests were conducted using coin cells (CR2032) and performed with a SINOPRO MRX CT-4008T Battery Tester. Celgard® 2400 was used as the separator, cut into 19 mm-diameter disks. The Si and graphite anode materials were dried under vacuum at 110 °C for 12 hours. The electrolyte composition consisted of 1.2 M lithium hexafluorophosphate in a mixture of ethylene carbonate and ethyl methyl carbonate (3 : 7 by volume), with a 10% volume addition of fluoroethylene carbonate; this electrolyte was sourced from Dongwha Electrolyte. As TM salts, Ni(II) acetylacetonate ($Ni(acac)_2$, Sigma-Aldrich), Co(II) acetylacetonate ($Co(acac)_2$, Sigma-Aldrich), Mn(II) acetylacetonate ($Mn(acac)_2$, Sigma-Aldrich), and Fe(II) acetylacetonate ($Fe(acac)_2$, Sigma-Aldrich) were used and they were dried under vacuum at 150 °C for 24 hours and then mixed with the electrolyte. The concentration of TM salt included in the electrolyte was set at 10 mM, 30 mM, and 50 mM. Each test utilized 100 μl of electrolyte.

For chronoamperometry test, graphite and Si pellets were prepared by mixing the respective powders with 1 wt% PTFE, followed by pelletization at 10 MPa for 10 minutes. To minimize contact resistance, silver paste was applied to both surfaces of the pellets, and measurements were performed using a holder setup. Chronoamperometry measurements were performed at a constant potential of 0.1 V for 5 hours. Over time, the current reached a steady-state saturation value. The electronic conductivity (σ) was calculated using the following equation:

$$\sigma = \frac{I \times d}{U \times A}$$

where I is the measured steady-state current, d is the thickness of the pellet, U is the applied potential (0.1 V), and A is the cross-sectional area of the pellet.

Table 1 Composition and characteristics of electrodes

		Gr	Si
Component, wt%	Wellcos natural graphite	80	—
	Kojundo korea Si	—	60
	Polyacrylic acid binder	10	10
	Super-P Li carbon black	10	30
Loading density, mg cm^{-2}		1.2	0.6
Disk size, mm		14	14

For cycle life test, the cells underwent a formation process of three cycles at a 0.05C rate. After formation, the cells were cycled at a 0.2C rate for 100 cycles for the cycle life test. For potentiostatic tests, the dModule 1A/20V Ivium-n-stat (Ivium) was used. All cells were discharged to 0.1 V at a 0.05C rate, then potentiostatic tests at 0.1 V were performed for 180 hours. The current was normalized to the lithiation capacity measured immediately before the potentiostatic hold test.

For postmortem analysis, all cell disassembly was done in an argon-filled glovebox. The electrodes were harvested and washed (for 1 minute each) in dimethyl carbonate (DMC).

X-ray photoelectron spectroscopy (XPS)

K-alpha+ (Thermofisher Scientific) was used for XPS. Air exposure to the samples was perfectly prevented because XPS equipment is attached to an argon-atmosphere glovebox. All data were calibrated to the C–C binding energy at 284.80 eV. XPS depth profiling was performed using C60+ ion sputtering. The Shirley background data were subtracted from all spectra. CasaXPS® was used for fitting, and the fitted data were extracted and plotted using Origin®. Relative atomic concentrations were calculated from the Gaussian fits.

Time-of-flight secondary ion mass spectrometry (ToF-SIMS)

A M6 (IONTOF GmbH) instrument was utilized for ToF-SIMS. Air exposure to the samples was minimized by mounting the samples onto a sample holder in argon-atmosphere glovebox and placing the sample holder with the samples in a vinyl pack filled and sealed with argon gas. The pack was then opened in a laboratory with relative humidity maintained below 15%. Within 15 seconds of opening the pack, the sample was transferred to the equipment load-lock chamber. The chamber reached a vacuum level lower than 10^{-6} mbar within 5 minutes. Depth profile analysis was composed of surface analysis in the negative polarity and subsequent sputtering. Bi_3^{2+} primary ions with an acceleration voltage of 30 keV and a pulsed beam current of 0.2 pA were used for analysis, and Cs^+ ions with an acceleration voltage of 1 keV and a beam current of 90 nA were used for sputtering. The areas of analysis and sputtering were 100 μm × 100 μm and 300 μm × 300 μm, respectively.

Inductively coupled plasma (ICP)

PTIMA 7300DV (PerkinElmer) was used for inductively coupled plasma optical emission spectroscopy (ICP-OES) and NexION 2000B (PerkinElmer) was used for inductively coupled plasma mass spectrometry (ICP-MS). The concentration of Mn ions at 10 mM on the graphite anode substrate was too low to be accurately measured using ICP-OES; hence, ICP-MS was employed for the analysis.

Data availability

The data supporting this article have been included as part of the ESI.†

Conflicts of interest

There are no conflicts to declare.

Acknowledgements

This research was supported by the Nano & Material Technology Development Program through the National Research Foundation of Korea (NRF) funded by Ministry of Science and ICT (RS-2024-00408823). This research was also supported by the National Research Foundation of Korea Grant funded by the Korean Government (MSIT) (No. RS-2023-00211760). This research was also supported by the National Research Foundation of Korea Grant funded by the Korean Government (MSIT) (No. RS-2024-00404099). This work was supported by the Industrial Technology Innovation Program (No. RS-2024-00438337, 2410002316, Development of highly stable single-crystal cathode material (Ni > 96%) for high safety and improved cycle-life performance) funded By the Ministry of Trade, Industry & Energy (MOTIE, Korea).

References

1 J. Wandt, A. Freiberg, R. Thomas, Y. Gorlin, A. Siebel, R. Jung, H. A. Gasteiger and M. Tromp, *J. Mater. Chem. A*, 2016, **4**, 18300–18305.
2 C. Delacourt, A. Kwong, X. Liu, R. Qiao, W. Yang, P. Lu, S. Harris and V. Srinivasan, *J. Electrochem. Soc.*, 2013, **160**, A1099.
3 C. Zhan, J. Lu, A. Jeremy Kropf, T. Wu, A. N. Jansen, Y.-K. Sun, X. Qiu and K. Amine, *Nat. Commun.*, 2013, **4**, 2437.
4 W. Li, *J. Electrochem. Soc.*, 2020, **167**, 090514.
5 I. A. Shkrob, A. J. Kropf, T. W. Marin, Y. Li, O. G. Poluektov, J. Niklas and D. P. Abraham, *J. Phys. Chem. C*, 2014, **118**, 24335–24348.
6 S. R. Gowda, K. G. Gallagher, J. R. Croy, M. Bettge, M. M. Thackeray and M. Balasubramanian, *Phys. Chem. Chem. Phys.*, 2014, **16**, 6898–6902.
7 G. G. Amatucci, A. Blyr, C. Sigala, P. Alfonse and J. M. Tarascon, *Solid State Ionics*, 1997, **104**, 13–25.
8 Y. K. Sun, K. J. Hong and J. Prakash, *J. Electrochem. Soc.*, 2003, **150**, A970.
9 M. M. Thackeray, C. S. Johnson, J. S. Kim, K. C. Lauzze, J. T. Vaughey, N. Dietz, D. Abraham, S. A. Hackney, W. Zeltner and M. A. Anderson, *Electrochem. Commun.*, 2003, **5**, 752–758.
10 J. S. Kim, C. S. Johnson, J. T. Vaughey, S. A. Hackney, K. A. Walz, W. A. Zeltner, M. A. Anderson and M. M. Thackeray, *J. Electrochem. Soc.*, 2004, **151**, A1755.
11 Z. Zhang, Z. Gong and Y. Yang, *J. Phys. Chem. B*, 2004, **108**, 17546–17552.
12 J.-M. Han, S.-T. Myung and Y.-K. Sun, *J. Electrochem. Soc.*, 2006, **153**, A1290.
13 S. S. Zhang, K. Xu and T. R. Jow, *J. Solid State Electrochem.*, 2003, **7**, 492–496.
14 A. Banerjee, B. Ziv, Y. Shilina, S. Luski, D. Aurbach and I. C. Halalay, *ACS Energy Lett.*, 2017, **2**, 2388–2393.
15 M. Ochida, Y. Domi, T. Doi, S. Tsubouchi, H. Nakagawa, T. Yamanaka, T. Abe and Z. Ogumi, *J. Electrochem. Soc.*, 2012, **159**, A961.
16 C. Zhan, T. Wu, J. Lu and K. Amine, *Energy Environ. Sci.*, 2018, **11**, 243–257.
17 S. Jurng, S. K. Heiskanen, K. K. Chandrasiri, M. Y. Abeywardana and B. L. Lucht, *J. Electrochem. Soc.*, 2019, **166**, A2721.
18 M. Obrovac and L. Krause, *J. Electrochem. Soc.*, 2006, **154**, A103.
19 M. Kim, S. P. Harvey, Z. Huey, S.-D. Han, C.-S. Jiang, S.-B. Son, Z. Yang and I. Bloom, *Energy Storage Mater.*, 2023, **55**, 436–444.
20 S. G. Yoon, K. H. Lee and M. Kim, *Appl. Phys. Lett.*, 2022, **121**, 200503.
21 M. Kim, Z. Yang, S. E. Trask and I. Bloom, *ACS Appl. Mater. Interfaces*, 2022, **14**, 15103–15111.
22 M. Kim, Z. Yang, S.-B. Son, S. E. Trask, A. Jansen and I. Bloom, *J. Mater. Chem. A*, 2021, **9**, 26904–26916.
23 V. Meunier, M. L. De Souza, M. Morcrette and A. Grimaud, *J. Electrochem. Soc.*, 2022, **169**, 070506.
24 L. Zhao, O. O. Capraz and N. R. Sottos, *ACS Appl. Energy Mater.*, 2024, **7**, 2142–2152.
25 D. H. Jang, Y. J. Shin and S. M. Oh, *J. Electrochem. Soc.*, 1996, **143**, 2204–2211.
26 R. J. Gummow, A. de Kock and M. M. Thackeray, *Solid State Ionics*, 1994, **69**, 59–67.
27 Y. Terada, Y. Nishiwaki, I. Nakai and F. Nishikawa, *J. Power Sources*, 2001, **97–98**, 420–422.
28 Y. Xia, Y. Zhou and M. Yoshio, *J. Electrochem. Soc.*, 1997, **144**, 2593–2600.
29 A. Blyr, A. Du Pasquier, G. Amatucci and J. M. Tarascon, *Ionics*, 1997, **3**, 321–331.
30 Z.-Y. Wu, Y.-Q. Lu, J.-T. Li, S. Zanna, A. Seyeux, L. Huang, S.-G. Sun, P. Marcus and J. Światowska, *ACS Omega*, 2021, **6**, 27335–27350.
31 X.-B. Cheng, C. Yan, X. Chen, C. Guan, J.-Q. Huang, H.-J. Peng, R. Zhang, S.-T. Yang and Q. Zhang, *Chem*, 2017, **2**, 258–270.
32 R. Sim, L. Su, A. Dolocan and A. Manthiram, *Adv. Mater.*, 2024, **36**, 2311573.
33 K. Schroder, J. Alvarado, T. A. Yersak, J. Li, N. Dudney, L. J. Webb, Y. S. Meng and K. J. Stevenson, *Chem. Mater.*, 2015, **27**, 5531–5542.
34 N. Schulz, R. Hausbrand, C. Wittich, L. Dimesso and W. Jaegermann, *J. Electrochem. Soc.*, 2018, **165**, A833.
35 C. Charton, J. Santos-Peña, A. Biller, E. De Vito, H. Galiano, M. Le Digabel and D. Lemordant, *J. Electrochem. Soc.*, 2017, **164**, A1454.
36 K. N. Wood and G. Teeter, *ACS Appl. Energy Mater.*, 2018, **1**, 4493–4504.
37 F. Ding, W. Xu, X. Chen, J. Zhang, M. H. Engelhard, Y. Zhang, B. R. Johnson, J. V. Crum, T. A. Blake and X. Liu, *J. Electrochem. Soc.*, 2013, **160**, A1894.
38 Q. Li, X. Liu, X. Han, Y. Xiang, G. Zhong, J. Wang, B. Zheng, J. Zhou and Y. Yang, *ACS Appl. Mater. Interfaces*, 2019, **11**, 14066–14075.

39 S. Lux, I. Lucas, E. Pollak, S. Passerini, M. Winter and R. Kostecki, *Electrochem. Commun.*, 2012, **14**, 47–50.
40 M. C. Schulze, M.-T. F. Rodrigues, J. D. McBrayer, D. P. Abraham, C. A. Apblett, I. Bloom, Z. Chen, A. M. Colclasure, A. R. Dunlop, C. Fang, K. L. Harrison, G. Liu, S. D. Minteer, N. R. Neale, D. Robertson, A. P. Tornheim, S. E. Trask, G. M. Veith, A. Verma, Z. Yang and C. Johnson, *J. Electrochem. Soc.*, 2022, **169**, 050531.
41 A. Verma, M. C. Schulze, A. Colclasure, M.-T. F. Rodrigues, S. E. Trask, K. Pupek and D. P. Abraham, *J. Electrochem. Soc.*, 2024, **171**, 070539.
42 J. D. McBrayer, K. L. Harrison, E. Allcorn and S. D. Minteer, *Front. Batter. Electrochem.*, 2023, **2**, 1308127.
43 H. Gao, L. Xiao, I. Plümel, G.-L. Xu, Y. Ren, X. Zuo, Y. Liu, C. Schulz, H. Wiggers and K. Amine, *Nano Lett.*, 2017, **17**, 1512–1519.